

Active Carpets in floating viscous films

Felipe A. Barros,^{1,*} Hugo N. Ulloa,^{2,†} Gabriel Aguayo,^{3,‡} Arnold J. T. M. Mathijssen,^{4,§} and Francisca Guzmán-Lastra^{5,¶}

¹*Departamento de Física, Facultad de Ciencias, Universidad de Concepción, Concepción, Chile*

²*Department of Earth and Environmental Science, University of Pennsylvania, Philadelphia, USA*

³*Departamento de Física, Facultad de Ciencias Físicas y Matemáticas, Universidad de Chile, Santiago Chile*

⁴*Department of Physics and Astronomy, University of Pennsylvania, Philadelphia, USA*

⁵*Departamento de Física, Facultad de Ciencias, Universidad de Chile, Santiago, Chile*

(Dated: April 12, 2024)

Earth's aquatic environments are inherently stratified layered systems where interfaces between layers serve as ecological niches for microbial swimmers, forming colonies known as *Active Carpets*. Previous theoretical studies have explored the hydrodynamic fluctuations exerted by *Active Carpets* in semi-infinite fluid media, demonstrating their capability to enhance thermal diffusion and mass transport in aquatic systems. Yet, little is understood about the fluid dynamics and impact of *Active Carpets* residing in confined layered environments, like slicks floating on water bodies. In this study, we report novel solutions for the hydrodynamic fluctuations induced by *Active Carpets* geometrically confined between a free surface and a fluid-fluid interface characterized by a jump in fluid viscosity. Combining theory and numerical experiments, we investigate the topology of the biogenic hydrodynamic fluctuations in a confined, thin fluid environment. We reveal that within this thin layer, *Active Carpets* gives shape to three characteristic regions: Region I is the closest zone to the *Active Carpet* and the fluid-fluid interface, where hydrodynamic fluctuations are dominantly vertical; Region II is further up from the *Active Carpet* and is characterized by isotropic hydrodynamic fluctuations; Region III is the furthest region, near the free surface and is dominated by horizontal flow fluctuations. We demonstrate that the extent of these regions depends strongly on the degree of confinement, i.e. the layer thickness and the strength of the viscosity jump. Lastly, we show that confinement fosters the emergence of large-scale flow structures within the layer housing the *Active Carpets*—not previously reported. Our findings shed light on the complex interplay between confinement and hydrodynamics in floating viscous film biological systems, providing valuable insights with implications spanning from ecological conservation to bio-inspired engineering.

I. INTRODUCTION

Microbial swimmers are ubiquitous across Earth's aquatic landscapes [1]. They thrive from wet surfaces to abyssal oceans, enduring extremes from freezing to boiling waters [2–4]. Microswimmers are finely equipped with an array of skills and taxes enabling them to navigate towards optimal regions or niches [e.g., 5, 6], where they harness chemical compounds and sunlight to synthesize their own food, forming colonies known as '*Active Carpets*' [7, 8]. These ecological niches of optimal food uptake and growth are usually found near the interface between two layers. For instance, photosynthetic microbes habit around the thermocline, the zone of maximum vertical temperature gradient in the water column, separating the upper warmer layer from the deeper, nutrient-enriched colder layer [6, 9, 10]. Microbial swimmers have adapted to the inherently layered nature of aquatic environments, where physical, chemical, and biological properties undergo a gradient in the direction of gravity. These layers can arise from various abrupt changes in fluid properties, including temperature (thermocline), salinity (haloclines), density (pycnoclines), dissolved oxygen (oxycline), dissolved chemicals (chemoclines), or sharp shifts in viscosity [11, 12]. Moreover, most of Earth's aquatic systems are capped by the air-

water interface, the free surface, where the atmosphere meets waters or thin oil films or slicks lying on top of water. Such a layering environment creates a wide range of niches for microbial swimmers and inert suspended matter [13–16], as well as vertical confinement that may control the ability of microbes to harvest food and self-clean via collective hydrodynamic fluctuations. Biogenic hydrodynamic stirring has been proved to enhance active diffusion [17–24], generate persistent flows for feeding processes in collective and single microswimmers [25–27], produce aggregation [28–33] and induce long-range hydrodynamic fluctuations [8]. *Active Carpets* formed by Stokeslets living close to non-slip boundaries drive non-equilibrium diffusion that drive an active diffusion much larger than thermal Brownian motion [7, 8]. Moreover, the diffusion is tensorial, with a vertical diffusion larger than horizontal diffusion, and it produces non-equilibrium transport that does not follow the Boltzmann distribution. Aguayo *et al.* [29] recently studied the hydrodynamic fluctuations induced by *Active Carpets* formed by dipole microswimmers organized into a thin layer beneath the free surface of a semi-infinite homogeneous fluid. The authors found that the hydrodynamics fluctuations produce anisotropic diffusion that decays slowly with distance, showing a remarkable biogenic long-range effect on vertical transport.

Vertical transport is essential for mixing and ventilation in stratified environments. A long-debated question is whether swimming organisms contribute to such processes in aquatic systems [34, 35]. To uncover the role of microorganisms in stratified liquid systems, Ardekani and Stocker [36] employed the multipole expansion technique to examine a single microswimmer, known as a stratlet. According to the bio-

* fbarros2017@udec.cl

† ulloa@sas.upenn.edu

‡ g.aguayo07@gmail.com

§ amaths@sas.upenn.edu

¶ fguzman@uchile.cl

physics operating at the micro-scale, the stratlet model considers an organism moving at low Reynolds numbers, $Re \ll 1$, in which viscous forces dominate over inertial ones. Their findings revealed that pullers moving in a stratified fluid do not generate persistent flows conducive to vertical mixing. Instead, they induce in-plane flows that strengthen the existing stratification. Theoretical studies further corroborated these findings, demonstrating that at low- Re , a single microbe swimming perpendicular to isopycnals has minimal impact on mixing [37]. Yet, numerical and laboratory experiments have demonstrated that the collective vertical migration of small organisms—like zooplankton swimming at intermediate Reynolds number $Re \sim O(1)$ [38, 39]—can drive a significant enhancement of the transport and mixing across fluid-fluid interfaces [40, 41]. Moreover, recently, it has been theoretically predicted that *Active Carpets* formed by large numbers of organisms swimming at low- Re can drive long-range hydrodynamic fluctuations that enhance transport in homogenous fluid environments. This prompts us to delve into the behavior of hydrodynamic fluctuations driven by *Active Carpets* within layered environments.

This manuscript focuses on *Active Carpets* living within a confined layer, bounded above by a free surface (air-water interface) and below by a fluid-fluid interface characterized by a viscosity interface that separates two fluid layers of viscosities μ_1 and μ_2 , as illustrated Fig. 1(a). Within this environment, an *Active Carpet* experiences two confining mechanisms: geometrical confinement, characterized by the thickness of the upper layer H (the floating film), and viscous confinement, characterized by the viscosity jump or ratio $\lambda = \mu_2/\mu_1$. We can posit two scenarios for λ . In a first scenario, $\lambda < 1$, the *Active Carpet* lives in a fluid that it is more viscous than its underlying layer. Whereas in the second scenario, $\lambda > 1$, the *Active Carpet* lives in a less viscous layer than the subject layer. In this case, λ tells us how soft ($\lambda \rightarrow 1$) or rigid ($\lambda \rightarrow \infty$) the fluid-fluid viscous interface is.

Recent research has studied the microorganisms' optimal swimming behavior in viscosity gradients (viscotaxis), revealing divergent trends. In some cases, microorganisms prefer swimming in low-viscosity regions, while in others, they favor high-viscosity environments [6, 42–45]. For instance, the *Chlamydomonas reinhardtii*, a type of phytoplankton, shows viscophobic behavior by forming thin layers near interfaces with $\lambda < 1$ [46]. Building upon the framework of *Active Carpets* [7, 8], we explore theoretically and numerically the impact of confinement on hydrodynamic fluctuations resulting from the collective swimming of organisms forming an *Active Carpet* residing at the upper vicinity of a viscosity interface.

In Section II, we introduce the mathematical model for both a single swimmer moving at low- Re and an *Active Carpet* in a layered environment. We explain the numerical modeling approach and parameters in Section III. In Section IV, we present and discuss our main findings, comprising new analytical solutions for *Active Carpets* in a layered aquatic environment, analyses of the topology of hydrodynamic fluctuations and the evidence of large-scale flow patterns driven by the *Active Carpet* within the layered system. Our study aims to shed light on the complex interplay between confinement and hydro-

drodynamics in these intriguing biological systems.

II. MATHEMATICAL MODEL

A. A microswimmer in a layered environment

We model the flow field of a single flagellated microswimmer moving in a homogeneous fluid of viscosity μ_1 , confined between two non-deforming boundaries [12, 47]. Here, the top boundary is a free surface interface, whereas the bottom is a fluid-fluid interface, where below it there is a second fluid of viscosity μ_2 . The ratio between both fluid viscosities is denoted as $\lambda = \mu_2/\mu_1$. The distance between both interfaces is H and is referred to as the film thickness.

The low Reynolds number regime describes the fluid motion driven by microscopic swimmers. In this regime, viscous forces are larger than inertial ones [48, 49]. Here, hydrodynamics flows are governed by the incompressible Stokes equations [50]. For a point force $\mathbf{F} = \mathbf{f}\delta(\mathbf{r} - \mathbf{r}_s)$ acting at $\mathbf{r}_s = (x_s, y_s, z_s)$ on a stationary fluid of dynamic viscosity μ we have

$$\nabla p(\mathbf{r}) - \mu \nabla^2 \mathbf{u}(\mathbf{r}) = \mathbf{F} \quad (1a)$$

$$\nabla \cdot \mathbf{u}(\mathbf{r}) = 0 \quad (1b)$$

where $\mathbf{u}(\mathbf{r})$ and $p(\mathbf{r})$ are the fluid velocity and pressure fields at position $\mathbf{r} = (x, y, z)$, respectively. The solution of Eqs. (1) in the absence of boundaries is well-known as the Stokeslet [51–53]

$$\mathbf{u}(\mathbf{r}, \mathbf{r}_s) = \frac{\mathcal{G}_{ij}(\mathbf{r}, \mathbf{r}_s) \cdot \mathbf{F}}{8\pi\mu}, \quad \mathcal{G}_{ij}(\mathbf{r}, \mathbf{r}_s) = \left(\frac{\delta_{ij}}{|\mathbf{d}|} + \frac{d_i d_j}{|\mathbf{d}|^3} \right), \quad (2)$$

where $\mathbf{d} = \mathbf{r} - \mathbf{r}_s$ is the relative position of the swimmer to the fluid. Derivatives of the Stokeslet are also solutions [54–56]. For swimming microorganisms, where the thrust and the drag force balance, the Stresslet is the first dominant term in the multipole expansion to describe their far-field flow [57].

Next, we include the boundaries. Following Desai and Ardekani [12], we construct the first approximation to the image system for the flow field produced by a microswimmer confined between a fluid-fluid interface and a free surface interface, as shown in Fig. 1(b).

The Stokes equations for a point force acting on fluid 1 are

$$-\nabla p^{(1)} + \mu_1 \nabla^2 \mathbf{u}^{(1)} + \mathbf{F} = 0, \quad (3a)$$

$$\nabla \cdot \mathbf{u}^{(1)} = 0, \quad (3b)$$

while for fluid 2 are

$$-\nabla p^{(2)} + \mu_2 \nabla^2 \mathbf{u}^{(2)} = 0, \quad (4a)$$

$$\nabla \cdot \mathbf{u}^{(2)} = 0. \quad (4b)$$

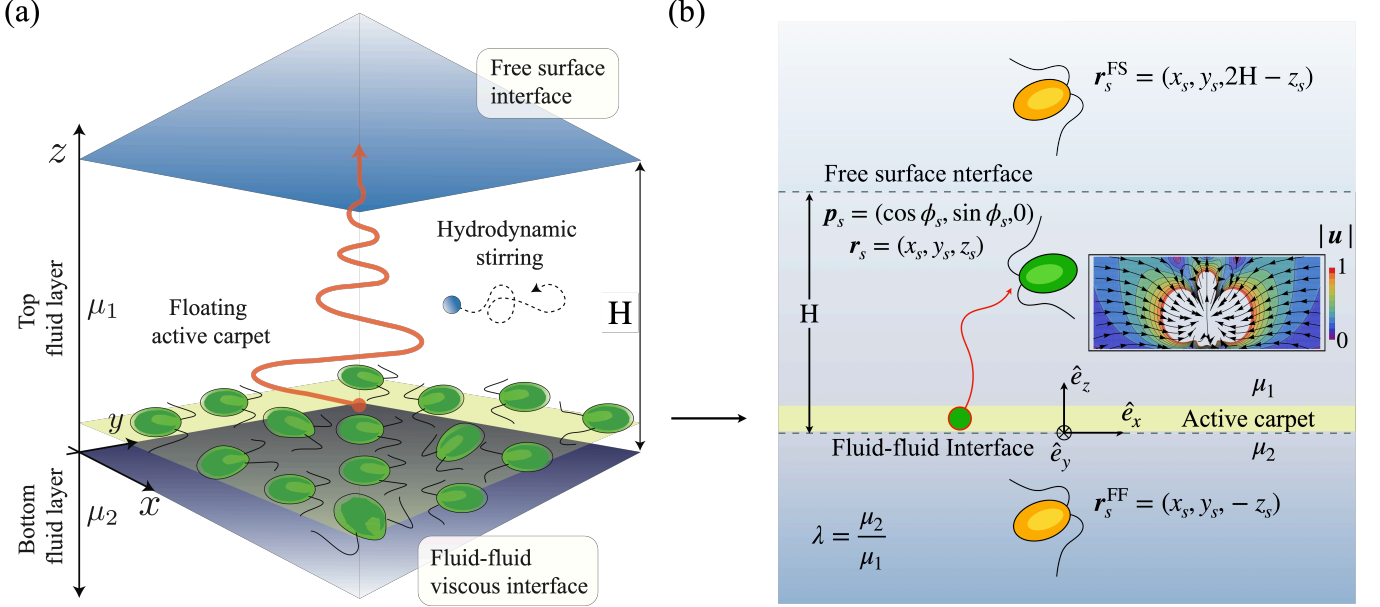


FIG. 1. (a) Schematic of a confined *Active Carpet* (yellow) formed by microswimmers living at a fixed distance σ from the bottom fluid-fluid interface (in green). The microswimmers stir their surrounding confined fluid (orange arrows). The ratio between fluid viscosities is $\lambda = \mu_2/\mu_1$. (b) Conceptual model for a single microswimmer confined between the parallel free surface interface and the fluid-fluid interface. Microorganisms swim in the x - y plane at $z = \sigma$. (c,d) Velocity field induced by a microorganism in the fluid of viscosity μ_1 . The first is a top-view projection in the x - y plane, and the second is a front-view in the x - y plane.

The velocity field of both fluids must satisfy the following boundary conditions at the fluid-fluid interface [47],

$$u_\alpha^{(1)} = u_\alpha^{(2)}, \text{ at } z = 0 \quad (5a)$$

$$u_z^{(1)} = u_z^{(2)} = 0, \quad (5b)$$

$$\mu_1 \left(\frac{\partial u_\alpha^{(1)}}{\partial z} + \frac{\partial u_z^{(1)}}{\partial \alpha} \right) = \mu_2 \left(\frac{\partial u_\alpha^{(2)}}{\partial z} + \frac{\partial u_z^{(2)}}{\partial \alpha} \right) \text{ at } z = 0, \quad (5c)$$

where $\alpha = x, y$, while at the free surface interface,

$$u_z^{(1)} = 0, \text{ at } z = H, \quad (6a)$$

$$\frac{\partial u_\alpha^{(1)}}{\partial z} + \frac{\partial u_z^{(1)}}{\partial \alpha} = 0, \text{ at } z = H. \quad (6b)$$

From solving (3) to (5), the image's system for an interface between two fluids of different viscosities leads to a generalization of the Blake tensor [47]

$$\begin{aligned} \mathcal{A}_{ij}(\mathbf{r}) = & \left(\frac{1-\lambda}{1+\lambda} \delta_{j\alpha} \delta_{\alpha k} - \delta_{j3} \delta_{3k} \right) \mathcal{G}_{ik}(\mathbf{r}) \\ & + \frac{2\lambda}{\lambda+1} h(\delta_{j\alpha} \delta_{\alpha k} - \delta_{j3} \delta_{3k}) \frac{\partial}{\partial r_k} \left(\frac{hr_i}{r^3} + \mathcal{G}_{i3}(\mathbf{r}) \right). \end{aligned} \quad (7)$$

For $\lambda = 0$, we recover the image flow field of a point force close to a free surface,

$$\mathcal{F}_{ij}(\mathbf{r}) = \mathcal{M}_{jk} \mathcal{G}_{ik}(\mathbf{r}), \quad (8)$$

where \mathcal{M}_{jk} is a mirror matrix, $\mathcal{M} = \text{diag}(1, 1, -1)$. This image system corresponds to the one satisfying the boundary condition at $z = H$.

Formally, a point force $\mathbf{F} = \mathbf{f} \delta(\mathbf{r} - \mathbf{r}_s)$ is acting at position $\mathbf{r}_s = (x_s, y_s, z_s)$. The image system to account for the fluid-fluid interface will be the one from Eq. (7), located at position $\mathbf{r}_s^{\text{FF}} = (x_s, y_s, -z_s)$. On the other hand, to account for the free surface interface we set a mirror image from Eq. (8) at position $\mathbf{r}_s^{\text{FS}} = (x_s, y_s, 2H - z_s)$. The velocity field produced by a point force parallel to both interfaces is given by

$$\begin{aligned} \mathbf{u}(\mathbf{r}, \mathbf{r}_s, \lambda, H) = & \mathcal{G}(\mathbf{r}, \mathbf{r}_s) \cdot \mathbf{f}_{\parallel} \\ & + (\mathcal{F}(\mathbf{r}, \mathbf{r}_s^{\text{FS}}, H) + \mathcal{A}(\mathbf{r}, \mathbf{r}_s^{\text{FF}}, \lambda)) \cdot \mathbf{f}_{\parallel}, \end{aligned}$$

where the second term is the full image system added to satisfy the induced hydrodynamic boundary conditions and $\mathbf{f}_{\parallel} = \mathbf{f}/(8\pi\mu_1)$ is the scaled force.

As shown in Fig. 1(b), because of the linearity of the Stokes equations, we use the same image system for expressing the velocity field of a force dipole with orientation \mathbf{p}_s ,

$$\mathbf{u}_D(\mathbf{r}, \mathbf{r}_s, \mathbf{p}_s) = \kappa(\mathbf{p}_s \cdot \nabla_s)[(\mathcal{G} + \mathcal{F} + \mathcal{A}) \cdot \mathbf{p}_s], \quad (9)$$

where derivatives $\nabla_s = \partial/\partial \mathbf{r}_s$ are taken with respect to the microswimmer's position. Here, $\kappa = f_{\parallel} \sigma/\mu_1$ corresponds to the dipolar strength, which characterizes the hydrodynamic distortions of each microswimmer and sets the timescale of the biogenically driven flow, $\tau = \sigma^3/\kappa$, with σ the microswimmer body length. On the one hand when $\kappa > 0$, the microswimmer generates an extensile flow (pusher) similar to motile bacteria powered by a helical flagella bundle. On the

other hand when $\kappa < 0$, the flow field is contractile (puller) similar to the flow generated by green microalgae *Chlamydomonas reinhardtii*, which forms thin phytoplankton layers in aquatic environments [6].

In nature, sharp vertical temperature gradients or the presence of natural and artificial oils can lead to sharp contrasts in fluid viscosity; especially at the skin of surface waters [58]. Also, during blooms, planktonic microorganisms have been reported to increase the effective ambient viscosity, generating strong viscosity gradients with relative viscosities $1 \lesssim \lambda \lesssim 3$ at short distances [59]. On the contrary, bacterial suspension has been proved to decrease ambient viscosity, depending on their concentration [60], with relative viscosities $O(10^{-3}) \lesssim \lambda \lesssim O(1)$.

In this study, we utilize the leading-order image system to describe far-field flows [12]. It is important to note that when two image flow fields are added to the hydrodynamic system, boundary conditions are only partially satisfied. To mitigate this discrepancy, recursive images of the original images must be added. However, since the first images closely approximate the confined natural system under investigation, they encapsulate most of the relevant physics. Subsequent images will inevitably be farther removed from the system [26].

As an example, the flow field generated, in the x - z plane, by a single puller microswimmer in a film of thickness $H = 3$, with $\kappa = 30$, the dipole strength of a flagellated microswimmer moving in water reported by Drescher et al. [61], and viscosity ratio $\lambda = 1.5$ – computed from Eq. (9) – is shown in the inset of Figs. 1(b). Streamlines show the typical trajectories followed by fluid parcels around this type of swimmer close to surfaces [26, 61]; contours show the intensity of the velocity field, this being more intense close to the singularity (white) and weaker far from it (purple).

B. Active Carpet in a layered aquatic environment

Our model considers a collection of dipole microswimmers constricted to move in the x - y plane at a fixed height $z = \sigma$, which corresponds to microswimmers moving above the viscosity interface forming the so-called Active Carpet, as sketched in Figs. 1(a). The Active Carpet is constituted of a dense suspension of microorganisms, each of them inhabiting this environment at positions $\mathbf{r}_s = (x_s, y_s, \sigma)$ and orientations $\mathbf{p}_s = (p_x, p_y, 0)$. We consider them in a stroboscopic diffusive regime [8, 29] such that as time progresses, all microswimmers are uniformly distributed in space and orientations in a 2D surface. Each microorganism stirs and energizes the confined water film, driving a flow field given by Eq. (9). Here, we probe the biogenically driven flow at positions $\mathbf{r}_0 = (x_0, y_0, z_0)$, corresponding to a fluid parcel between the free surface and fluid-fluid interface. To find a far-field approximation for probe fluid parcels far from the Active Carpet, we performed a Taylor expansion for the flow field generated by a single microswimmer, such that $z_s = \epsilon z$ with $\epsilon \ll 1$. With this analytical expression, we can measure different statistical properties of the collectively generated flow.

The mean flow field averaged over a finite carpet of size R

with microswimmer uniformly distributed in cylindrical coordinates, ρ_s , θ_s and orientations ϕ_s is

$$\langle \mathbf{v}(\mathbf{r}) \rangle = \int \mathbf{u}(\mathbf{r}, \mathbf{r}_s, \mathbf{p}_s) \mathcal{F}(\mathbf{r}_s, \mathbf{p}_s) d\mathbf{r}_s d\mathbf{p}_s, \quad (10)$$

where $\mathcal{F} = n/2\pi > 0$ is a uniform distribution of swimmers for a carpet number density n and $\langle \cdot \rangle$ is the average over the collection of swimmers. Here $\mathbf{r}_s = (\rho_s \cos \theta_s, \rho_s \sin \theta_s, \sigma)$ is the swimmer's position and $\mathbf{p}_s = (\cos \phi_s, \sin \phi_s, 0)$ the swimmer's orientation, with $\phi_s, \theta_s \in [-\pi, \pi]$. Such a carpet is able to generate a mean flow field that attracts suspended particles [7]. However, when the carpet size increases significantly, i.e. $R \rightarrow \infty$, the mean flow converges to zero [8]. Here, we consider an infinite carpet, so that $\langle \mathbf{v}(\mathbf{r}) \rangle = 0$. Yet, the variance $\mathcal{V}_{ij} = \langle v_i v_j \rangle$ is different from zero, where $i, j = x, y, z$ denote its components in cartesian coordinates. The variance, which encapsulates what we call fluctuations, governs the active diffusion process that tracer particles experience over the carpet; its magnitude depends strongly on the geometry of the environment and can be computed analytically using the following expression for the variance tensor

$$\mathcal{V}_{ij} = \langle v_i v_j \rangle = \int u_i u_j \mathcal{F} d\mathbf{r}_s d\mathbf{p}_s. \quad (11)$$

In addition, we define the average vorticity field induced by the confined Active Carpet as

$$\langle \boldsymbol{\omega} \rangle = \langle \nabla \times \mathbf{v} \rangle = \int (\nabla \times \mathbf{u}) \mathcal{F} d\mathbf{r}_s d\mathbf{p}_s. \quad (12)$$

We now turn the focus to the numerical framework utilized to simulate the dynamics of confined Active Carpet.

III. NUMERICAL SIMULATIONS

As discussed in Section II B, we do not follow each microswimmer's trajectory in time. Instead, we investigate the effects of the Active Carpet in the surrounding fluid once microswimmers have passed from the ballistic regime to a diffusive regime [see e.g. 8, 29]. In brief, we model Active Carpets through the Fast Dynamics Framework. The Fast Dynamics Framework is made by randomly distributing $N_s = 10^5$ microswimmers with positions $\mathbf{r}_s = (x_i, y_i, \sigma)$ and orientations $\mathbf{p}_s = (\cos \phi_i, \sin \phi_i, 0)$, with $\phi_i \in [-\pi, \pi]$, $i \in [1, N_s]$ in a finite square domain, $L \times L$, where L is the size of the Active Carpet. The microswimmers number density in the Active Carpet is defined as $n = N_s/(2L)^2$. Both the positions and orientations are uniformly distributed. The total flow generated by the active carpet is computed by superposing the flow velocity of each individual microswimmer given by Eq. (9). Thus, the collective velocity field driven by the ensemble, or the colony, is determined by

$$\mathbf{v}(\mathbf{r}, \mathbf{r}_s, \mathbf{p}_s) = \sum_{i=1}^{N_s} \mathbf{u}_D(\mathbf{r}, \mathbf{r}_s, \mathbf{p}_s). \quad (13)$$

This velocity is then computed for an ensemble of N_e independent *Active Carpet* configurations. Hence, we compute the ensemble variance tensor of the flow field Eq. (13), as defined in Eq. (11), averaging over a finite number of *Active Carpet* ensembles N_e . Using this framework, we investigate the dynamics of passive tracer particles stirred by the collective action of the colony. A tracer particle, with position $\mathbf{r}^T(\tau_e)$, feels the aggregated flow exerted by the *Active Carpet* ensemble and reacts to changes in the re-orientation microswimmers experience as time progresses; τ_e is the dimensionless time. As a result, passive tracer dynamics are governed by the following equation [8, 29, 54, 62]

$$\frac{d\mathbf{r}^T(\tau_e)}{d\tau_e} = \mathbf{v}(\mathbf{r}^T, \mathbf{r}_s, \mathbf{p}_s). \quad (14)$$

As illustrated in Fig. 1(a), we explore tracer particle dynamics between the *Active Carpet* and the surface interface, $\sigma < \mathbf{r}^T(\tau_e) < H$. We integrate Eq. (14) numerically utilizing an Euler scheme, with a nondimensional integration time step $\Delta t = 10^{-3}$. At each time step, the tracer particle excursions a length $\Delta \mathbf{r}^T$ determined by a new random independent *Active Carpet* ensemble.

The size of the *Active Carpet* is crucial in computing every observable within this framework. Mathijssen *et al.* [7] stressed that if the *Active Carpet* is too small, a drift flow can overpower the motion of tracer particles. To mitigate this effect, we ensure that the *Active Carpet* is sufficiently long so that tracer trajectories are controlled by the biogenically driven fluid flow [7, 8, 29].

In this study, we set the following parameters unless otherwise stated: dipole strength $\kappa = -30$ following [63], *Active Carpet* number density $n = 0.1$, vertical position in the far-field approximation $\sigma = 1$, small parameter $\epsilon = 0.1$, ensemble

number $N_e = 10^3$, and *Active Carpet* length $L = 10^4$. Our primary focus is investigating the impact of confinement size H and interface strength λ . In what follows, we explore how the degree of fluid confinement impacts the spatial characteristics of the hydrodynamic stirring driven by *Active Carpets*.

IV. RESULTS AND DISCUSSION

A. Fluctuation and dispersion of tracer particles

We first characterize the hydrodynamic fluctuations driven by the confined *Active Carpet* whose members swim parallel to the boundary interfaces, as sketched in Fig. 1(a). To this point, the theory developed by Mathijssen *et al.* [7] allows us to directly compute the variance Eq. (11) of the flow field Eq. (9) by performing a far-field approximation of the flow field (Section II B). Note that off-diagonal components of the variance tensor vanish. Additionally, by symmetry, we have that $\langle v_x^2 \rangle = \langle v_y^2 \rangle$ [8]. Therefore we do have only two fluctuations to characterize, the horizontal $\langle v_x \rangle$ and the vertical one, $\langle v_z \rangle$.

As a consequence of the confined geometry and the boundary conditions, the velocity field and its variance depend upon the ratio $\lambda = \mu_2/\mu_1$, characterizing the viscous interface, the thickness of the aquatic film H , as well as the intrinsic physical and geometrical parameters of the Stokes solution and far-field approximation. Hence, each variance component is a function of $\langle v_i^2 \rangle = \langle v_i^2 \rangle(n, \kappa, \sigma, \lambda, \epsilon, H, z_0)$, where z_0 is the height of a fluid parcel relative to the *Active Carpet*. The obtained analytical expressions are

$$\begin{aligned} \langle v_x^2 \rangle = & \frac{\pi \kappa^2 n}{64} \left(\frac{21\sigma^2 \epsilon^2 - 22\sigma \epsilon (z_0 - 2H) + 11(z_0 - 2H)^2}{(z_0 - 2H)^4} + \frac{336\sigma^2 \lambda^2 \epsilon^2}{(\lambda + 1)^2 z_0^4} + \frac{160\sigma \lambda \epsilon}{(\lambda + 1)^2 z_0^3} \right. \\ & + \frac{36z_0(8\sigma \lambda \epsilon (H + 2\sigma \epsilon) + H(2H + 3\sigma \epsilon))}{H^5(\lambda + 1)} - \frac{36z_0^2(2\sigma \lambda \epsilon (2H + 5\sigma \epsilon) + H(H + 2\sigma \epsilon))}{H^6(\lambda + 1)} \\ & \left. + \frac{8H(H + \sigma \epsilon) - 32\sigma \lambda \epsilon (2H + 3\sigma \epsilon)}{H^4(\lambda + 1)} + \frac{44}{(\lambda + 1)^2 z_0^2} \right), \end{aligned} \quad (15a)$$

$$\begin{aligned} \langle v_z^2 \rangle = & \frac{9\pi \kappa^2 n}{32} \left(\frac{2\sigma^2 \epsilon^2 - 2\sigma \epsilon (z_0 - 2H) + (z_0 - 2H)^2}{(z_0 - 2H)^4} + \frac{80\sigma^2 \lambda^2 \epsilon^2}{(\lambda + 1)^2 z_0^4} + \frac{32\sigma \lambda \epsilon}{(\lambda + 1)^2 z_0^3} \right. \\ & - \frac{4z_0(8\sigma \lambda \epsilon (H + 2\sigma \epsilon) + H(2H + 3\sigma \epsilon))}{H^5(\lambda + 1)} + \frac{4z_0^2(2\sigma \lambda \epsilon (2H + 5\sigma \epsilon) + H(H + 2\sigma \epsilon))}{H^6(\lambda + 1)} \\ & \left. + \frac{4}{(\lambda + 1)^2 z_0^2} \right). \end{aligned} \quad (15b)$$

Note that $\epsilon \ll 1$ but not zero. The limit $\epsilon \rightarrow 0$ does not have a physical interpretation. To validate these analytical results we

performed simulations using Eq. (13) to obtain numerically the total velocity field averaged over N_e of *Active Carpet* en-

sembles (Section III). From numerical results, we computed the variance for a set of z_0 values within the range (σ, H) , where we set the body length σ as the unit of length through our results.

Fig. 2(a) presents the analytical and simulation results for $\lambda = 1.5$ and $H = 40$. First, the theory and simulations show great agreement. Second, the effect of confinement in the biogenically driven fluid flow is severe. As the plot shows, horizontal and vertical fluctuations cross at a particular height, which we denote as $z_0 = z_*$. We found that vertical variances are more significant than horizontal ones for almost half the film thickness, $z_0 \propto 0.43H$. Using Eqs. (15a) and (15b) we can determine exactly that they cross at height $z_* = 16.6$ (represented by the yellow star on the plot); here, we expect the fluctuations to have the same strength. To achieve this, horizontal fluctuations become more significant than for heights closer to the Active Carpet, $z_0 < z_*$. According to this unique feature, we can separate the space into three regions, denoted by I, II, and III. Region I represents the range of heights where vertical fluctuations dominate over horizontal fluctuations, Region II represents the locus where fluctuations are isotropic, whereas Region III represents the range of heights where horizontal fluctuations dominate over vertical fluctuations. To illustrate this feature, the inset shows results of fluctuations for different values of λ in the list $[0.1, 0.5, 1.5]$ (dashes, dotted and dot-dash, respectively) and a film thickness $H = 20$. The variance curves intersect in the same fashion. Results show that the cross-point z_* varies depending on the value of λ . Smaller values of λ lead cross-points closer to the top free surface, and the contrary happens for greater values, i.e. the cross-point gets closer to the Active Carpet.

Our results contrast significantly with previous studies of *Active Carpets*. In the case of Guzmán-Lastra *et al.* [8], in which the authors investigated *Active Carpets* living near a no-slip surface, the fluctuations decay monotonically as $\langle v_i^2 \rangle \propto z_0^{-4}$ for parallel dipoles. Similarly, Aguayo *et al.* [29] found that fluctuations were long-ranged, with $\langle v_i^2 \rangle \propto z_0^{-2}$ in the case of a free surface. In our case, the hydrodynamic fluctuations decay in a more complex manner as a result of the confinement and the influence of the viscous fluid-fluid interface. Although all the variances maintain their anisotropic behavior, we observe a non-monotonic trend, with a striking change in the amplitude of the variance components and the dominance of directional effects. Indeed, at some distance z_* , the vertical fluctuations decay much more rapidly with z_0 than the horizontal fluctuations as we go farther from the *Active Carpet*. Therefore, characterizing the locus z_* and its dependence on the parameters controlling the degree of confinement is essential since it determines where fluctuations and the flow direction become spatially biased.

We carried out simulations using Eq. (14) to prove that the anisotropic behavior of fluctuations effectively impacts surrounding tracer particles depending on the region where they move. For this, we created an *Active Carpet* with $N_s = 10^5$ microswimmers and $L = 1.5 \times 10^4$. The *Active Carpet* was confined within a film of thickness $H = 40$, and the bottom interface was characterized by a viscosity ratio to $\lambda = 1.5$. From the analytical solution Eq. (15), we deter-

mined the intersection height z_* by resolving the equation $\langle v_x^2 \rangle(z_*) = \langle v_z^2 \rangle(z_*)$. Once determined z_* , we seeded passive tracers at a height $z_0 = 27.7 > z_*$ to measure vertical-dominated motions, at a height $z_0 = z_*$ to measure isotropic motions, and a height $z_0 = 10 < z_*$ to measure horizontal-dominated motion. Then, we simulated $\tau_e = 180$ time steps by numerically integrating Eq. (14). This time was enough to determine the characteristic topology of the space through which tracers are transported by the hydrodynamic fluctuations. The latter was obtained by averaging the displacement \bar{d}_i for all tracer particles in every direction \hat{e}_i , $i = x, y, z$. The ellipsoids in Fig. 2(b) (scaled for visualization) show the resulting topology for each region. Thus, we confirm that tracer particles have a more prominent vertical motion at heights $z_0 < z_*$ (red) closer to the Active Carpet, equal to horizontal motions at $z_0 = z_*$ (ginger) and that horizontal motions become dominant at $z_0 > z_*$ (green). This particular example demonstrating a zonification of the hydrodynamic fluctuations across the fluid layer raises more general questions. How does the degree of confinement, determined by H and λ , impact the geometry of the biogenically driven hydrodynamic fluctuations? And how does z_* change in terms of λ and H ?

B. Impact of confinement on fluctuation's geometry

We explore answers to the above questions by examining how z_* depends upon the film's thickness H and the viscous fluid-fluid interface, λ . Fig. 2 shows us a significant anisotropy and non-monotonic behavior of the hydrodynamic fluctuations induced by the confined *Active Carpet*. A major result is that we found the existence of three regions whose spatial distribution is determined by z_* ; the height above the *Active Carpet* at which the vertical and horizontal variance of the velocity fluctuations equal, heights z lower than z_* where vertical fluctuations dominate over horizontal fluctuations, and heights between z_* and H , horizontal fluctuations dominate over vertical fluctuations. The analytical solution Eq. (15) reported in Section IV A enables us to describe and analysis these three regions change as function of H and λ .

We computed $z_*(\lambda, H)$ for a wide range of film's thicknesses, varying H two order of magnitude, and varying the viscous fluid-fluid interface ratio λ over a range that could potentially be observed in aquatic environments. For this, we resolve numerically the nonlinear equation for $\langle v_x^2 \rangle(z, H, \lambda) - \langle v_z^2 \rangle(z, H, \lambda) = 0$ for $z \in (\sigma, H)$. The root of this equation corresponds to z_* .

Fig. 3(a) shows the dependency of z_* on the film's thickness H for five values of $\lambda \in [0, 4]$. First, we identify that z_* increases monotonically with $10 \leq H \leq 100$. This implies that thicker aquatic films create conditions for isotropic fluctuations to be further away from the *Active Carpet*, i.e. the region where vertical fluctuations dominate over horizontal fluctuations also expands monotonically with H . From an ecological viewpoint, this is relevant since the *Active Carpet* can have longer range for both attracting or repelling mass. Second, we observe that z_* is larger for smaller λ . In other words, the more viscous is the layer where the *Active Car-*

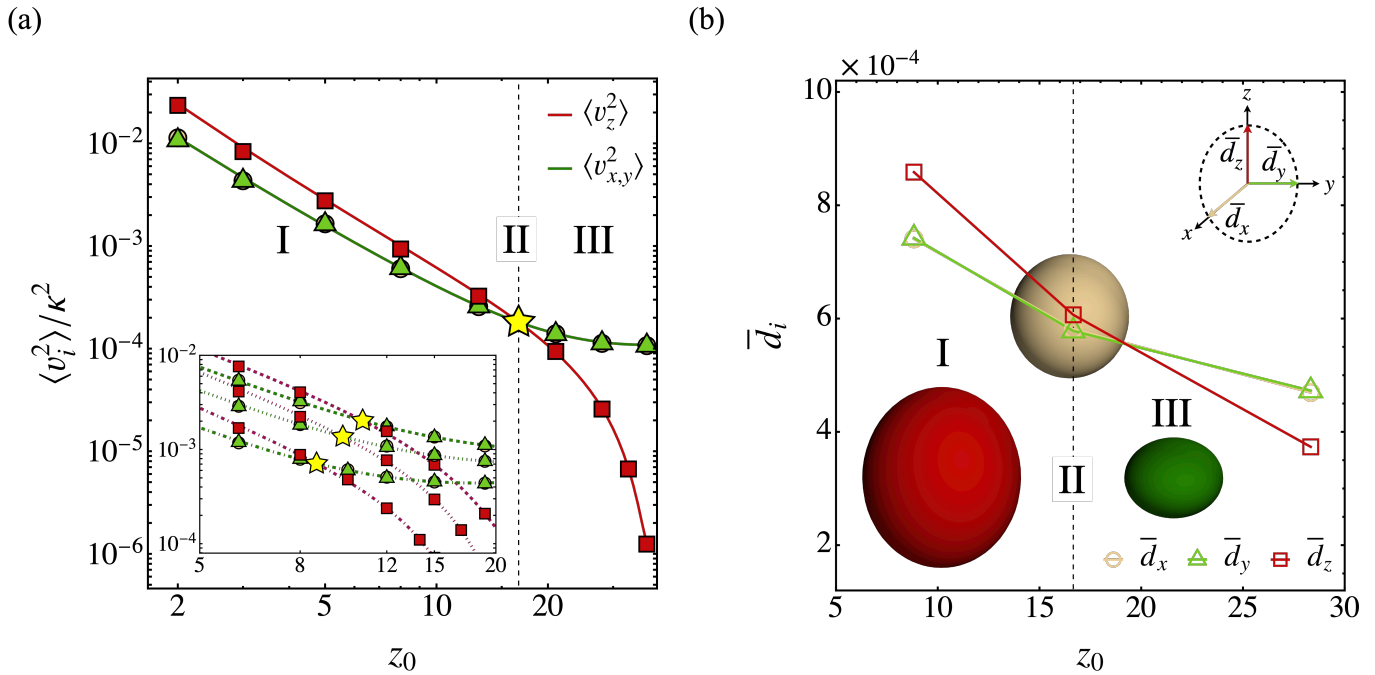


FIG. 2. Anisotropic diffusion driven by *Active Carpets*. (a) Variance of the hydrodynamic fluctuations driven by an *Active Carpet* in the horizontal and vertical directions (green, red solid lines), as defined in Eqs. (11). Markers are simulation points obtained from Eq. (13). The star marks the intersection between theoretical variances $\langle v_z^2 \rangle(z_*) = \langle v_{x,y}^2 \rangle(z_*)$. Regions I, II and III indicate the dominance of fluctuations according to the distance from the *Active Carpet*. Here $H = 40$ and $\lambda = 1.5$. Inset: Theoretical variances for $H = 20$, and three different values of λ , $\lambda = 0.1, 0.5, 1.5$, denoted by dashed, dotted and dash-dotted lines, respectively. Stars are cross-points. (b) Ellipsoids represent the average displacement of tracer particles computed from Eq. (14) for each fluctuation region. In green, tracer particles start at $z_0 < z_*$, while in red, they start at $z_0 < z_* < H$. In ginger, they start exactly at $z_0 = z_*$.

pet habits, the longer is the extent of the region where vertical fluctuations dominate over horizontal fluctuations. For the extreme case of $\lambda \rightarrow 0$, the fluid where the *Active Carpet* inhabits is dramatically more viscous than the fluid below the *Active Carpet*, $\mu_1 \gg \mu_2$.

Such a big difference in viscosity can be observed in fresh and marine aquatic environments, where algae blooms change the physico-chemical properties of a region in water column [64]. At some point, this dramatic spatial changes in viscosity push the fluid away from the Newtonian limit. Nonetheless, Newtonian rheology remains a fair approximation for gently varying fluid viscosity, as the case of liquid water [65]. For $\lambda = 0$, and the range of H values here explore, we obtain that $z_* = 0.55H$. Whereas for a slightly larger value, $\lambda = 0.5$, we obtain that $z_* = H/2$. We show that with low λ values, the system is at a sort of local equilibrium phase of the hydrodynamics fluctuations effects. This means that fluctuations regions I and III will have almost of the same extent. At larger values of λ , the proportionality we just described changes. Fig. 3(a) shows a different result for $\lambda = 4$, where we find that in average, $z_* = 0.35H$. Here, we are strengthening the interface by making λ larger; from our framework, one would expect to recover a well-studied hydrodynamic system, a free-surface liquid film held by a rigid surface for $\lambda \gg 1$ [26]. As a result, we observe that for larger λ the hydrodynamic fluctuations are, on average, more planar-directed motions than

vertical motions since the region dominated by vertical fluctuations reduces to 35% of the film's thickness, i.e. horizontal fluctuations dominate over 75% of the film. From these results, it is apparent that λ plays a major role in unbalancing the system and changing the architecture of the hydrodynamic fluctuations so that the confined *Active Carpet* may promote, for example, biogenic mass reorganization mechanisms such as aggregation, recently investigated in a semi-infinite fluid [29].

Fig. 3(b) illustrates the relationship between z_* and λ within the range $\lambda \in [0, 4]$, considering different film thicknesses ($20 \leq H \leq 100$). Notably, the graph reveals that z_* decreases with increasing λ , indicating that stiffer fluid-fluid interfaces promote the expansion of Region III, where horizontal fluctuations outweigh vertical ones. This behavior mirrors the viscous control observed in analogous scenarios, such as superconfined subsurface faults, where viscosity drives fluid flow fluctuations towards quasi-two-dimensional states [66]. Furthermore, our findings indicate that variations in H exert a more pronounced effect on z_* at lower λ values. Specifically, in thin water films ($H = 20$), z_* exhibits weak sensitivity to changes in the strength of the fluid-fluid interface characterized by λ . Conversely, as the film thickness increases, z_* becomes significantly more responsive to variations in λ .

Fig. 3(c) serves as a comprehensive summary of our findings, encapsulating the essence of our investigation. This fig-

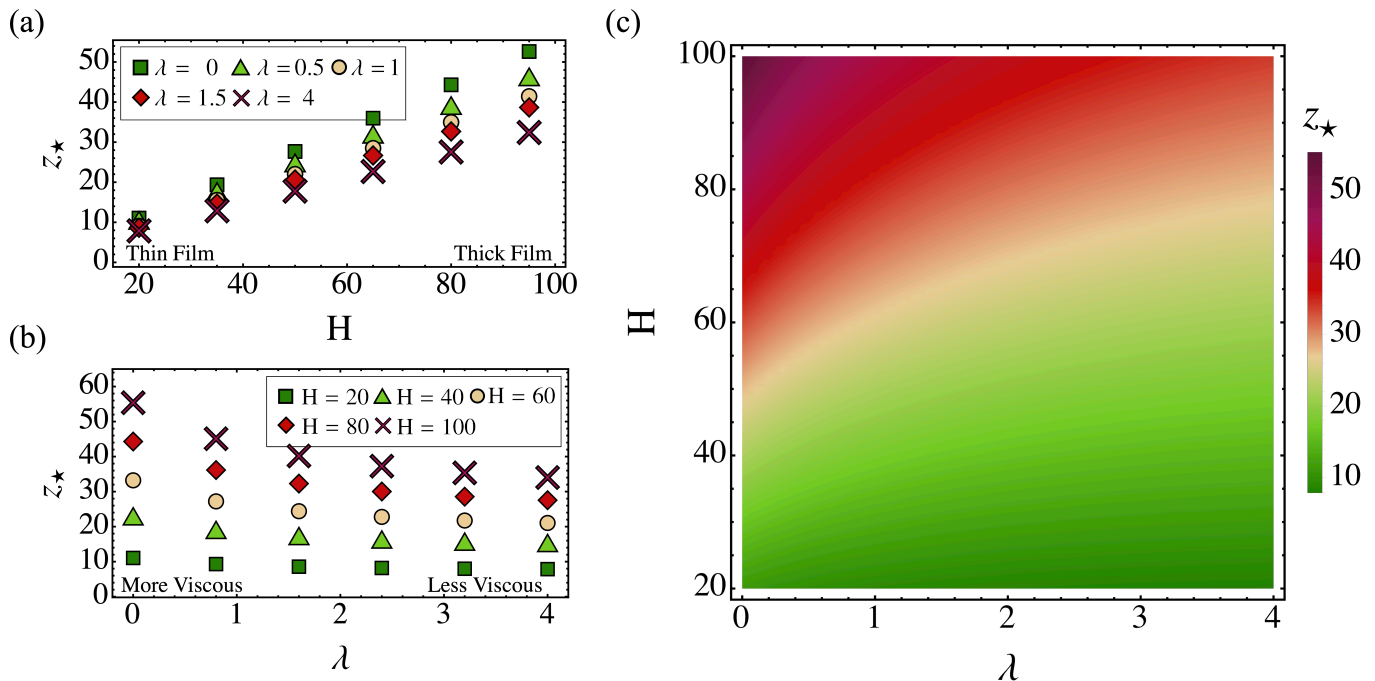


FIG. 3. The impact of confinement of the flow structure driven by *Active Carpets*. Shown are analytical solutions for the cross-point height z_* for a domain of the parameters λ and H . In (a) from thin (small H) to thick films (large H), and in (b) more viscous floating film ($\lambda < 1$) to less viscous floating film ($\lambda > 1$). In (c), the full dependence is shown.

ure illustrates the surface representation of z_* , depicting its dependency on two pivotal factors: the geometrical confinement denoted by H and the viscous confinement quantified by the ratio λ . By integrating these parameters, the results effectively delineate the complex dynamics of hydrodynamic fluctuations across different regimes (I, II, III) within the film. It portrays the nonlinear relationship between z_* and the confinement parameters, offering valuable insights into the underlying mechanisms at play. The results in Fig. 3 underscore the tangible influence exerted by both geometrical and viscous confinements on the spatial structure of velocity fluctuations. This influence extends beyond mere fluctuations, wielding significant control over *Active Carpets* and shaping the trajectories followed by passive tracers. Consequently, an intriguing question arises: Could confined *Active Carpets* potentially catalyze the emergence of aggregated large-scale coherent flow patterns? To delve deeper into this quest, we next examine the coherence of fluid motions and patterns in space by means of pair correlation analysis, mean velocity, and vorticity fields.

C. Flow coherence and roll-like formation

A defining feature of living systems is their ability to induce mechanical disturbances on their surroundings over scales greater than their characteristic individual size, prompting investigations into their potential for enhancing mixing in aquatic environments. This capacity of swimming organisms in stirring fluids, particularly through interactions with

each other, has garnered significant attention in recent years [19, 21, 22, 24, 40, 67, 68]. In the case of microbes swimming in layered, stratified waters—characterized by sharp gradients in density—theoretical arguments suggest individual swimmers have low capacity to mix fluid [37, 69]. Yet, whether the collective action of small swimming organisms can significantly affect the functioning of the fluid environment remains an open debate [34, 35, 37]. This motivates our quest for collective effects on large-scale hydrodynamic structures driven by *Active Carpet* within confined layered aquatic systems. Pair velocity correlation emerges as a metric for understanding the relationships between fluid parcel dynamics and biogenic fluid perturbations [7, 28, 29].

We compute the spatial pair velocity correlation to examine how the geometrical and viscous confinement affects the coherence of the flow fluctuations driven by an *Active Carpet*, defined as

$$C_i(d_0) = \frac{\langle v_i(\mathbf{r}_1)v_i(\mathbf{r}_2) \rangle_e}{\sqrt{\langle v_i^2(\mathbf{r}_1) \rangle_e \langle v_i^2(\mathbf{r}_2) \rangle_e}}, \quad (16)$$

where $d_0 = |\mathbf{r}_2 - \mathbf{r}_1|$ is the Euclidean distance between two fluid parcels in position \mathbf{r}_1 and \mathbf{r}_2 with fixed height z_0 , above the *Active Carpet*. The operator $\langle \cdot \rangle_e$ represents an *Active Carpet* ensemble average, and the variance tensor Eq. (11) is utilized to compute the numerator in Eq. (16). We performed numerical simulations to compute Eq. (16) following the next steps. First, we evaluate the flow induced by the *Active Carpet* at $\mathbf{r}_{1,2} = (\pm d_0/\sqrt{2}, \pm d_0/\sqrt{2}, z_0)$ with $z_0 = 10$ for a wide range of distances $d_0 \in [0.01, 200]$. The flow is determined from Eq. (13) at positions $\mathbf{r}_{1,2}$; it results from a single

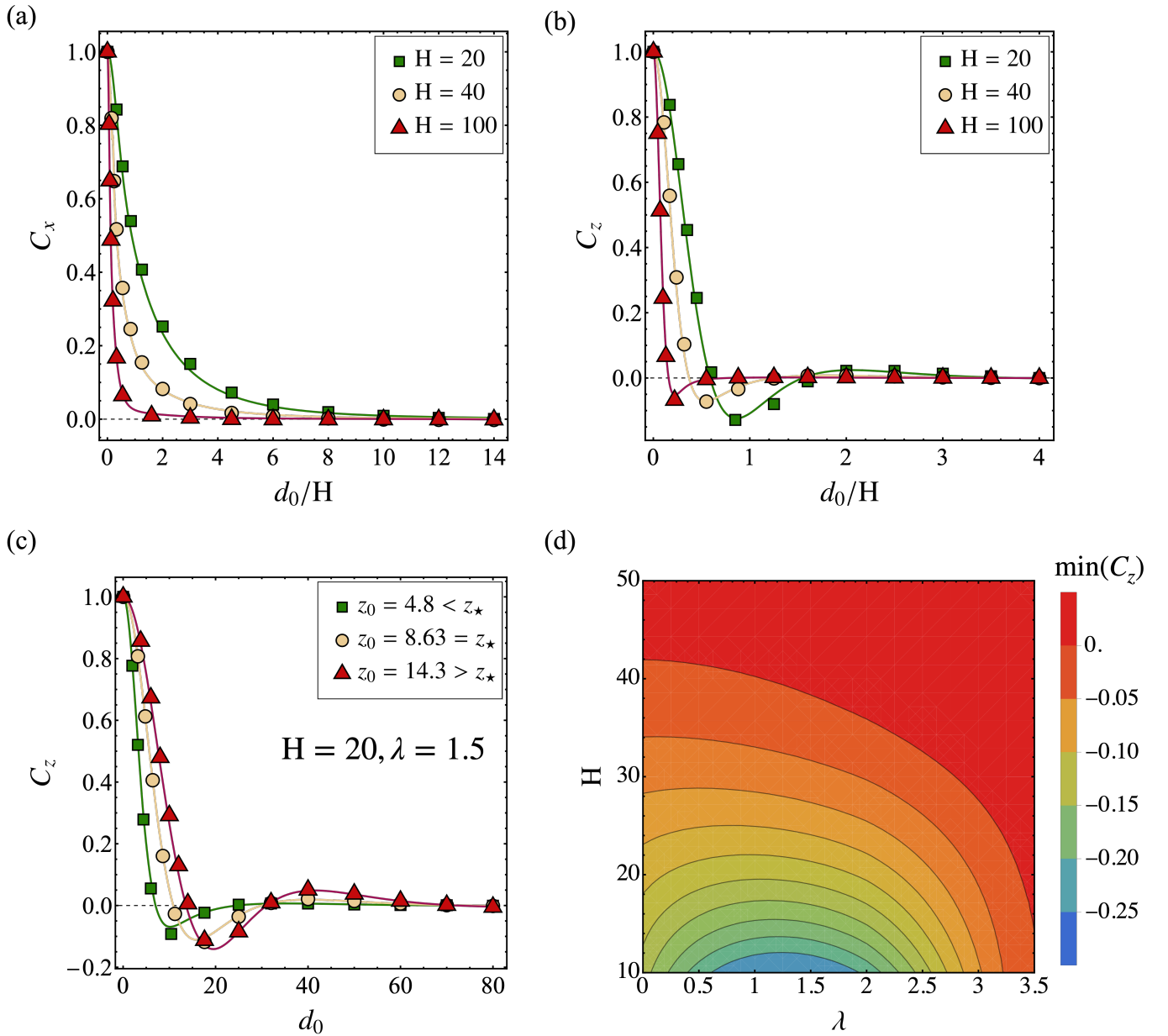


FIG. 4. Coherence of flows driven by *Active Carpets*. (a, b) Velocity pair correlation function to the relative distance between a pair of tracer particles, d_0 , normalized by the confinement size relative to the Active Carpet, for $\lambda = 1.5$, $\sigma = 1$, and $\kappa = -30$. Markers are simulation points. (c) Vertical velocity pair correlation function, for $H = 20$ and $\lambda = 1.5$ on z_0 values according to fluctuations regions. Markers are simulation points and solid lines correspond to semi-analytical solutions. (d) Phase diagram of vertical Correlation minima versus λ and H .

Active Carpet ensemble of length $L = 500$, using the far-field approximation for the flow field and $N = 10^5$ microswimmers, following Guzmán-Lastra *et al.* [8]. Then, we compute Eq. (16) for each ensemble and take the average over ensembles. Results are shown and discussed next.

Fig. 4(a) displays the pair correlation, C_x , in the \hat{e}_x direction, representing horizontal correlation, as a function of d_0/H . For simplicity, we omit results for \hat{e}_y , which is symmetric to those in \hat{e}_x . We examine the horizontal velocity pair correlation between particles separated by a distance d_0 for three H values ($H \in [20, 40, 100]$), with a fixed λ ($\lambda = 1.5$)

and a representative height $z_0 = 10$ above the Active Carpet. It is important to note that we normalize d_0 to the relative size of the film, H , to the *Active Carpet* to gauge the characteristic length of decorrelation relative to the film size. The varying H range allows us to observe that increasing geometrical confinement (i.e., thinner H) expands the relative extent of positively correlated tracer motions over distance d_0 . In simpler terms, the results indicate that horizontal flows exhibit slower decorrelation with increasing distance d_0 in more confined systems. This trend is evident when comparing the curves associated with high geometrical confinement ($H = 20$) and

less confinement ($H = 100$). This suggests that for an Active Carpet, disrupting fluid parcels parallel to it is challenging. This phenomenon may be attributed to coherent flows aligning with the constrained motion of microswimmers, resulting in biased, non-prominent horizontal flows. As a notable aside, our numerical findings align with the semi-analytical solution for $\langle v_i(\mathbf{r}_1)v_i(\mathbf{r}_2) \rangle = \int v_i(\mathbf{r}_1)v_i(\mathbf{r}_2)F d\mathbf{r}_s d\mathbf{p}_s$, shown by solid lines in Fig. 4.

Given that the confinement of *Active Carpets* primarily occurs in the \hat{e}_z direction, we delve deeper into the horizontal pair correlation in the \hat{e}_z direction, C_z , which we refer to as vertical pair correlation. The results, depicted in Fig. 4(b) for $\lambda = 1.5$, not only demonstrate good agreement between numerically obtained results (markers) and semi-analytical solutions (lines) but also reveal notable differences from horizontal pair correlation (C_x), as shown in Fig. 4(a).

An intriguing observation is the significantly shorter decorrelation distance for flow fluctuations in the vertical direction compared to horizontal fluctuations. This is evident from the distance $d_0/(H)$ over which the C_z and C_x curves decay to zero. The vertical pair correlation decays at least three times faster than the horizontal pair correlation, suggesting a distinct behavior. Moreover, a key difference is the occurrence of negative values in C_z , indicating flow fluctuations in opposite directions at specific distances d_0 . Such behavior is commonly associated with vortical flow structures, also observed in microswimmer's sheets, active turbulence experiments, and bacterial swarming [70–72].

In the most confined scenario examined here (see green squares in Fig. 4(b)), the curve reaches its minimum $\min(C_z)$ almost at $d_0 \approx H$, suggesting that vortex-like structures scale with the size of the geometrical confinement H . The emergence of such large-scale flow structures raises intriguing possibilities. For instance, microbial colonies formed by a monolayer of swimmers, resembling an Active Carpet, could potentially create coherent flow structures in the water column nearly 20 times their characteristic thickness under strong confinement.

In Section II B, we defined the region where active fluctuations exhibit a preferred direction. As this effect originates from the flow itself, we can thoroughly examine the vertical pair correlation C_z in detail. To illustrate how C_z changes at different heights, we fix the values of $H = 40$ and $\lambda = 1.5$ while varying the position z_0 at which flows are measured. The results presented in Fig. 4(c) demonstrate the sensitivity of C_z with respect to height above the *Active Carpet*. Firstly, notice we measure C_z as a function of d_0 . Interestingly, we observe similar trends to those depicted in Fig. 4(b), where the correlation reaches its minimum at a distance proportional to the size of confinement. This suggests that vertical fluctuations dominate within this region. Notably, the curves exhibit more fluctuations compared to the previous case, which could be attributed to increased confinement. This interpretation aligns with our previous observations.

We have highlighted that the vertical pair correlation reaches a minimum, indicating a region where fluid experiences vertical flow fluctuations in opposing directions. To further explore the intensity of this negative correlation, we

vary H and λ . Fig. 4(d) presents the minimum vertical pair correlation $\min(C_z)$ for $H \in [10, 50]$ and $\lambda \in [0, 3.5]$, computed using the semi-analytical approach. Our analysis reveals that the negative correlation, and thus the intensity of opposing flows, becomes stronger with increased geometrical confinement. Interestingly, we also observe that viscosity confinement, controlled by λ , enhances $\min(C_z)$ within the range $\lambda \in [0.5, 2]$. The nonmonotonic dependence with λ remains poorly understood at present, and this warrants future research for extreme conditions. In the limit of a non-slip boundary at the viscosity interface, i.e. $\lambda \rightarrow \infty$, we observe the pair correlations briefly cross the y -axis in the planar and vertical directions. The latter suggests the appearance of a weak complex flow structure related to the action of the *Active Carpet* and confinement. Conversely, in the case of a free-surface and unconfined aquatic environment, i.e. $\lambda \rightarrow 0$ and $H \rightarrow \infty$, the system does not show significant evidence of an emerging fluid flow structure. For a better understanding of the fluid dynamics of this asymptotic scenario, we refer the reader to Fortune *et al.* [73].

The question of whether confined fluid environments give rise to large-scale flow structures remains unanswered. In our study, we delve into the emergence of vortex-like patterns induced by confined *Active Carpets* by examining the spatial structure of the vertical velocity component and the flow vorticity. We investigate these quantities in a Cartesian coordinate system (x, y, z) to ensure clarity and guide our search for large-scale patterns amidst the biogenic flow fluctuations. In Fig. 5(a), we illustrate the velocity field v_z on the z - x plane, computed from Eq. (10) using a semi-analytical approach with a spatial resolution of $\Delta z = 0.5$ and $\Delta x = 0.5$. To highlight coherent trends, we show the sign of the vertical velocity component v_z , coloring upward motions in red (+1), downward motions in blue (-1), and no motion in white (0). The results reveal a consistent pattern, demonstrating coherence changes in the vertical flow direction with respect to x . Notably, the characteristic length of this ‘spatial wave pattern’ scales as H . In Fig. 5(b,c,d), we show the vorticity components $\omega_x, \omega_y, \omega_z$ on the x - z plane. Like panel (a), we represent the sign of ω_i to filter variability and identify large-scale structures and regions with equal vorticity direction. The findings confirm the existence of vortical flow patterns analogous to roll-like formations (exhibiting positive and negative vorticity), with their characteristic vortex length scaling with H , especially for ω_z and ω_y . Our results offer a glimpse into the ability of *Active Carpets* to drive large-scale flow structures in confined environments, bearing striking similarities to phenomena like bio-convection [19, 74], biogenic flows in extremely confined systems [72], thermally-driven convection in superconfined environments [75, 76], and kitchen flows [77]. Such confined flows, characterized by roll-like patterns, are renowned for their high mixing efficiency [19, 66]. In essence, our findings raise fundamental questions about the power of *Active Carpets* inhabiting layered environments to shape their surroundings, enhance the mixing of suspended and dissolved mass in aquatic environments, and facilitate transport between fluid-fluid interfaces and layers.

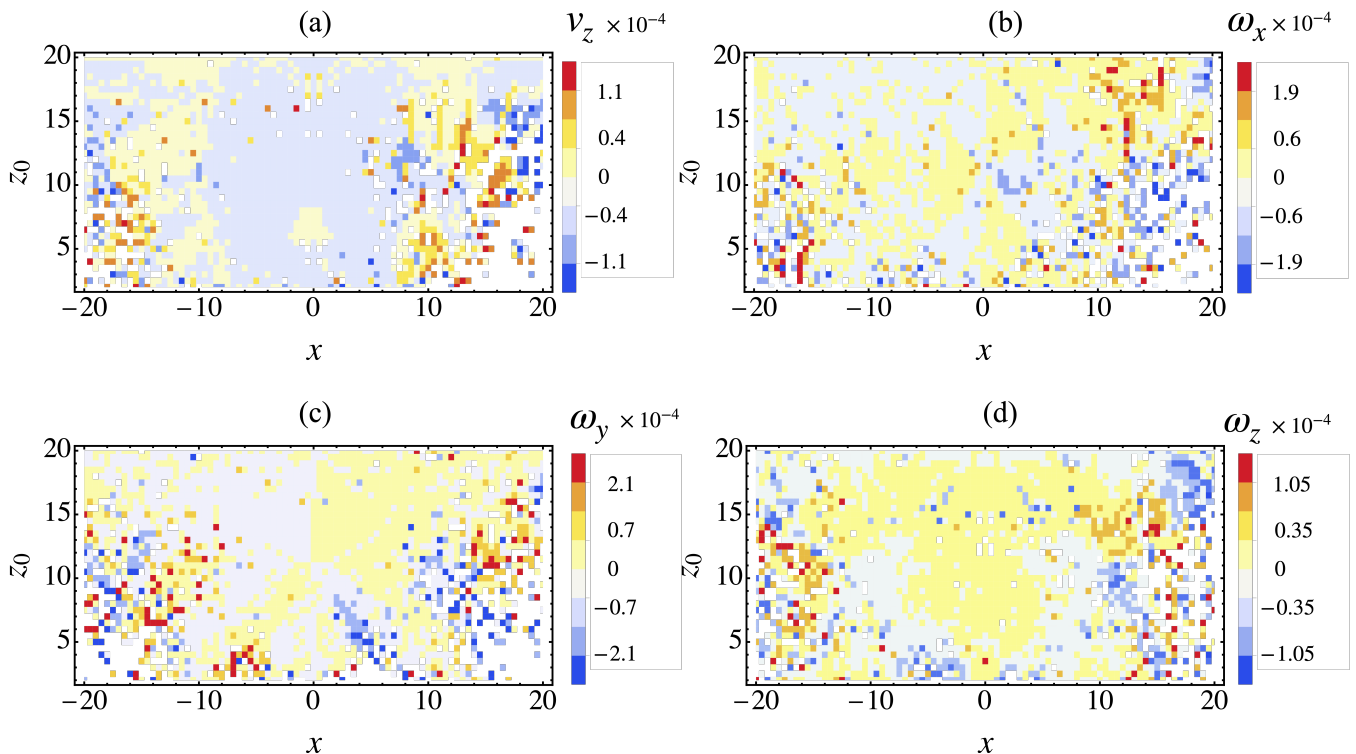


FIG. 5. *Active Carpets* can drive large scale recirculations. (a) Average vertical velocity exerted by an *Active Carpet* on fluid parcels across the confinement space, for $H = 20$, $\lambda = 1.5$, $\kappa = -30$, and $\sigma = 1$. (b,c,d) Vorticity field above the *Active Carpet* where Anti-clockwise (blue) and clockwise (yellow) vortical flows extend over space.

V. CONCLUSIONS

We have delved into the hydrodynamics of confined *Active Carpets* within layered aquatic systems. Our study is centered on three main aspects: (i) characterizing the spatial distribution of hydrodynamic fluctuations and the dispersion of passive tracers (Section IV A), (ii) assessing the influence of geometrical and viscous confinement on the hydrodynamics propelled by *Active Carpets* (Section IV B), and (iii) exploring the emergence of macroscopic hydrodynamic structures, referred to herein as roll-like formations (Section IV C). Our main findings read as follow:

1. We derive and report analytical expressions for the active flow fluctuations induced by *Active Carpets* confined in a layer of thickness H , between a free surface and a fluid-fluid interface characterized by a viscosity ratio. Our solutions reveal a pronounced non-monotonic behavior in the biogenic hydrodynamic fluctuations, particularly in the vertical direction. This characteristic contrasts with observations made in an *Active Carpet* near a single surface system [8, 29]. The non-monotonic dynamics of these hydrodynamic fluctuations are intricately influenced by the degree of geometrical and viscous confinement imposed by H and the viscosity ratio $\lambda = \mu_2/\mu_1$ at the fluid-fluid interface, where μ_1 is the viscosity of the fluid where the *Active Carpet* lives, and μ_2 is the viscosity of the deeper

layer. Numerical simulations corroborate the findings obtained from analytical solutions. These simulations provide a deeper exploration into the dynamics of passive tracer particles, showcasing the height-dependent topology of motions above the *Active Carpet*.

2. We show how the topology of hydrodynamic fluctuations undergoes transformation depending on the degree of geometrical confinement and the intensity of the viscosity ratio at the fluid-fluid interface boundary. Notably, we have uncovered the presence of three distinct spatial regions: (I) A proximal region to the *Active Carpet* where vertical fluctuations supersede horizontal fluctuations; (II) An intermediate region characterized by isotropic hydrodynamic fluctuations; and (III) The furthest region from the *Active Carpet* where horizontal fluctuations prevail over vertical fluctuations. This newfound understanding equips us with a tool to wield control over directed motion within confined vertical spaces. Furthermore, it illustrates how both dependencies are intrinsically linked to the amplification or diminishment of regions of agitation.
3. By measuring the velocity pair correlation of the exerted hydrodynamic fluctuations induced by the confined *Active Carpet*, we demonstrate the existence of coherent vortical motion predominantly propelled by vertical flows. Our investigation pinpointed that the

characteristic length of the formed roll-like patterns is intimately tied to the thickness of the confined layer harboring the *Active Carpet*. Remarkably, these coherent vortical structures manifest with exceptional prominence in highly confined systems and in the presence of sharp viscosity jumps at the fluid-fluid interface.

These findings carry implications for our comprehension of microbial swimmers that flourish and cultivate biofilms at interfaces in natural shallow water environments [12], such as (i) ponds etched upon soil and ice [78, 79], (ii) shallow saline lagoons and wetlands [80], (iii) streams [81], inside the human body [32, 82] and even in human habitats like the thin films of water found in kitchens, bathrooms, swimming pools and laboratories [83, 84].

By shedding light on the dynamics of these active flows, our research offers insights into the behavior of microbial communities in thin layers within aquatic ecosystems. From pristine natural settings to human-altered landscapes, the understand-

ing of the hydrodynamics induced by *Active Carpets* is crucial for devising strategies to manage and harness the potential of microbial populations for various applications, ranging from water remediation to microfluidics and biotechnology.

ACKNOWLEDGMENT

F.A.B., G.A. and F.G.-L. have received support from the ANID Millennium Science Initiative Program NCN19 170, Chile. F.G.-L. was supported by Fondecyt Iniciacin No. 11220683. H.N.U. and A.J.T.M.M. were supported by start-up grants from the University of Pennsylvania. A.J.T.M.M. acknowledges funding from the United States Department of Agriculture (USDA-NIFA AFRI grants 2020-67017-30776 and 2020-67015-32330), the Charles E. Kaufman Foundation (Early Investigator Research Award KA2022-129523) and the University of Pennsylvania (University Research Foundation Grant and Klein Family Social Justice Award).

-
- [1] E. Lauga and T. R. Powers, The hydrodynamics of swimming microorganisms, *Reports on progress in physics* **72**, 096601 (2009).
- [2] A. Dechesne, G. Wang, G. Gülez, D. Or, and B. F. Smets, Hydration-controlled bacterial motility and dispersal on surfaces, *Proceedings of the National Academy of Sciences* **107**, 14369 (2010).
- [3] C. Vetriani, J. W. Voordeckers, M. Crespo-Medina, C. E. O'Brien, D. Giovannelli, and R. A. Lutz, Deep-sea hydrothermal vent epsilonproteobacteria encode a conserved and widespread nitrate reduction pathway (nap), *The ISME journal* **8**, 1510 (2014).
- [4] E. L. Doting, M. B. Jensen, E. K. Peter, L. Ellegaard-Jensen, M. Tranter, L. G. Benning, M. Hansen, and A. M. Anesio, The exometabolome of microbial communities inhabiting bare ice surfaces on the southern greenland ice sheet, *Environmental Microbiology*, e16574 (2024).
- [5] A. Javadi, J. Arrieta, I. Tuval, and M. Polin, Photobioconvection: towards light control of flows in active suspensions, *Philosophical Transactions of the Royal Society A* **378**, 20190523 (2020).
- [6] W. M. Durham and R. Stocker, Thin phytoplankton layers: characteristics, mechanisms, and consequences, *Annual review of marine science* **4**, 177 (2012).
- [7] A. J. Mathijssen, F. Guzmán-Lastra, A. Kaiser, and H. Löwen, Nutrient transport driven by microbial active carpets, *Physical Review Letters* **121**, 248101 (2018).
- [8] F. Guzmán-Lastra, H. Löwen, and A. J. Mathijssen, Active carpets drive non-equilibrium diffusion and enhanced molecular fluxes, *Nature Communications* **12**, 1906 (2021).
- [9] J. Sharples, M. C. Moore, T. P. Rippeth, P. M. Holligan, D. J. Hydes, N. R. Fisher, and J. H. Simpson, Phytoplankton distribution and survival in the thermocline, *Limnology and Oceanography* **46**, 486 (2001).
- [10] B. Fernández Castro, O. Sepúlveda Steiner, D. Knapp, T. Posch, D. Bouffard, and A. Wüest, Inhibited vertical mixing and seasonal persistence of a thin cyanobacterial layer in a stratified lake, *Aquatic Sciences* **83**, 38 (2021).
- [11] R. Stocker, Marine microbes see a sea of gradients, *science* **338**, 628 (2012).
- [12] N. Desai and A. M. Ardekani, Biofilms at interfaces: microbial distribution in floating films, *Soft Matter* **16**, 1731 (2020).
- [13] A. Ahmadzadegan, S. Wang, P. P. Vlachos, and A. M. Ardekani, Hydrodynamic attraction of bacteria to gas and liquid interfaces, *Physical Review E* **100**, 062605 (2019).
- [14] J. Deng, M. Molaie, N. G. Chisholm, and K. J. Stebe, Motile bacteria at oil-water interfaces: *Pseudomonas aeruginosa*, *Langmuir* **36**, 6888 (2020).
- [15] G. Subbiahdoss and E. Reimhult, Biofilm formation at oil-water interfaces is not a simple function of bacterial hydrophobicity, *Colloids and Surfaces B: Biointerfaces* **194**, 111163 (2020).
- [16] L. Voskuhl and J. Rahlff, Natural and oil surface slicks as microbial habitats in marine systems: A mini review, *Frontiers in Marine Science* **9**, 1020843 (2022).
- [17] A. Morozov and D. Marenduzzo, Enhanced diffusion of tracer particles in dilute bacterial suspensions, *Soft Matter* **10**, 2748 (2014).
- [18] G. Miño, J. Dunstan, A. Rousselet, E. Clément, and R. Soto, Induced diffusion of tracers in a bacterial suspension: theory and experiments, *Journal of Fluid Mechanics* **729**, 423 (2013).
- [19] T. Sommer, F. Danza, J. Berg, A. Sengupta, G. Constantinescu, T. Tokyay, H. Bürgmann, Y. Dressler, O. Sepúlveda Steiner, C. Schubert, *et al.*, Bacteria-induced mixing in natural waters, *Geophysical Research Letters* **44**, 9424 (2017).
- [20] A. J. T. M. Mathijssen, R. Jeanneret, and M. Polin, Universal entrainment mechanism controls contact times with motile cells, *Phys. Rev. Fluids* **3**, 033103 (2018).
- [21] O. Sepúlveda Steiner, D. Bouffard, and A. Wüest, Persistence of bioconvection-induced mixed layers in a stratified lake, *Limnology and Oceanography* **66**, 1531 (2021).
- [22] S. Simoncelli, S. J. Thackeray, and D. J. Wain, On biogenic turbulence production and mixing from vertically migrating zooplankton in lakes, *Aquatic Sciences* **80**, 1 (2018).
- [23] R. Ran, Q. Brosseau, B. C. Blackwell, B. Qin, R. L. Winter, and P. E. Arratia, Bacteria hinder large-scale transport and enhance small-scale mixing in time-periodic flows, *Proceedings of the National Academy of Sciences* **118**, e2108548118 (2021).

- [24] J. Singh, A. E. Patteson, B. O. T. Maldonado, P. K. Purohit, and P. E. Arratia, Bacterial activity hinders particle sedimentation, *Soft Matter* **17**, 4151 (2021).
- [25] A. V. Kanale, F. Ling, H. Guo, S. Fürthauer, and E. Kanso, Spontaneous phase coordination and fluid pumping in model ciliary carpets, *Proceedings of the National Academy of Sciences* **119**, e2214413119 (2022).
- [26] A. J. Mathijssen, A. Doostmohammadi, J. M. Yeomans, and T. N. Shendruk, Hydrodynamics of micro-swimmers in films, *Journal of Fluid Mechanics* **806**, 35 (2016).
- [27] V. Škultéty, D. Bárdfalvy, J. Stenhammar, C. Nardini, and A. Morozov, Hydrodynamic instabilities in a 2-d sheet of microswimmers embedded in a 3-d fluid, arXiv:2302.13966 (2023).
- [28] S. Belan and M. Kardar, Pair dispersion in dilute suspension of active swimmers, *The Journal of Chemical Physics* **150** (2019).
- [29] G. Aguayo, A. J. Mathijssen, H. N. Ulloa, R. Soto, and F. Guzman-Lastra, Floating active carpets drive transport and aggregation in aquatic ecosystems, arXiv preprint arXiv:2312.11764 (2023).
- [30] S. Gokhale, J. Li, A. Solon, J. Gore, and N. Fakhri, Dynamic clustering of passive colloids in dense suspensions of motile bacteria, *Physical Review E* **105**, 054605 (2022).
- [31] P. Kushwaha, V. Semwal, S. Maity, S. Mishra, and V. Chikkadi, Phase separation of passive particles in active liquids, *Physical Review E* **108**, 034603 (2023).
- [32] A. J. Maheshwari, A. M. Sunol, E. Gonzalez, D. Endy, and R. N. Zia, Colloidal hydrodynamics of biological cells: A frontier spanning two fields, *Physical Review Fluids* **4**, 110506 (2019).
- [33] R. Großmann, L. S. Bort, T. Moldenhawer, M. Stange, S. S. Panah, R. Metzler, and C. Beta, Non-gaussian displacements in active transport on a carpet of motile cells, *Physical Review Letters* **132**, 088301 (2024).
- [34] S. Simoncelli, S. J. Thackeray, and D. J. Wain, Can small zooplankton mix lakes?, *Limnology and Oceanography Letters* **2**, 167 (2017).
- [35] E. Kunze, Biologically generated mixing in the ocean, *Annual review of marine science* **11**, 215 (2019).
- [36] A. Ardekani and R. Stocker, Stratlets: low reynolds number point-force solutions in a stratified fluid, *Physical review letters* **105**, 084502 (2010).
- [37] G. L. Wagner, W. R. Young, and E. Lauga, Mixing by microorganisms in stratified fluids, *Journal of Marine Research* **72**, 47 (2014).
- [38] S. Wang and A. M. Ardekani, Biogenic mixing induced by intermediate reynolds number swimming in stratified fluids, *Scientific reports* **5**, 17448 (2015).
- [39] D. Noto and H. N. Ulloa, Simple tracking of occluded self-propelled organisms, *Measurement Science and Technology* **35**, 035705 (2023).
- [40] I. A. Houghton, J. R. Koseff, S. G. Monismith, and J. O. Dabiri, Vertically migrating swimmers generate aggregation-scale eddies in a stratified column, *Nature* **556**, 497 (2018).
- [41] R. Ouillon, I. Houghton, J. Dabiri, and E. Meiburg, Active swimmers interacting with stratified fluids during collective vertical migration, *Journal of Fluid Mechanics* **902**, A23 (2020).
- [42] C. Datt and G. J. Elfring, Active particles in viscosity gradients, *Physical Review Letters* **123**, 158006 (2019).
- [43] B. Liebchen, P. Monderkamp, B. Ten Hagen, and H. Löwen, Viscotaxis: Microswimmer navigation in viscosity gradients, *Physical review letters* **120**, 208002 (2018).
- [44] V. A. Shaik and G. J. Elfring, Hydrodynamics of active particles in viscosity gradients, *Physical Review Fluids* **6**, 103103 (2021).
- [45] Marcos, H. C. Fu, T. R. Powers, and R. Stocker, Bacterial rheotaxis, *Proceedings of the National Academy of Sciences* **109**, 4780 (2012).
- [46] M. R. Stehnach, N. Waisbord, D. M. Walkama, and J. S. Guasto, Viscophobic turning dictates microalgae transport in viscosity gradients, *Nature Physics* **17**, 926 (2021).
- [47] K. Aderogba and J. Blake, Action of a force near the planar surface between two semi-infinite immiscible liquids at very low reynolds numbers, *Bulletin of the Australian Mathematical Society* **18**, 345 (1978).
- [48] G. I. Taylor, Analysis of the swimming of microscopic organisms, *Proceedings of the Royal Society of London. Series A. Mathematical and Physical Sciences* **209**, 447 (1951).
- [49] E. M. Purcell, Life at low reynolds number, *American journal of physics* **45**, 3 (1977).
- [50] G. G. Stokes *et al.*, *On the effect of the internal friction of fluids on the motion of pendulums* (Pitt Press Cambridge, 1851).
- [51] G. Hancock, The self-propulsion of microscopic organisms through liquids, *Proceedings of the Royal Society of London. Series A. Mathematical and Physical Sciences* **217**, 96 (1953).
- [52] J. Happel and H. Brenner, *Low Reynolds number hydrodynamics: with special applications to particulate media*, Vol. 1 (Springer Science & Business Media, 2012).
- [53] S. Kim and S. J. Karrila, *Microhydrodynamics: principles and selected applications* (Courier Corporation, 2013).
- [54] A. J. Mathijssen, D. O. Pushkin, and J. M. Yeomans, Tracer trajectories and displacement due to a micro-swimmer near a surface, *Journal of Fluid Mechanics* **773**, 498 (2015).
- [55] S. E. Spagnolie and E. Lauga, Hydrodynamics of self-propulsion near a boundary: predictions and accuracy of far-field approximations, *Journal of Fluid Mechanics* **700**, 105 (2012).
- [56] A. T. Chwang and T. Y.-T. Wu, Hydromechanics of low-reynolds-number flow. part 2. singularity method for stokes flows, *Journal of Fluid mechanics* **67**, 787 (1975).
- [57] G. Batchelor, The stress system in a suspension of force-free particles, *Journal of fluid mechanics* **41**, 545 (1970).
- [58] M. Hondzo, J. You, J. Taylor, G. Bartlet, and V. R. Voller, Measurement and scaling of lake surface skin temperatures, *Geophysical Research Letters* **49**, e2021GL093226 (2022).
- [59] Ö. Guadayol, T. Mendonca, M. Segura-Noguera, A. J. Wright, M. Tassieri, and S. Humphries, Microrheology reveals microscale viscosity gradients in planktonic systems, *Proceedings of the National Academy of Sciences* **118**, e2011389118 (2021).
- [60] V. A. Martinez, E. Clément, J. Arlt, C. Douarce, A. Dawson, J. Schwarz-Linek, A. K. Creppy, V. Škultéty, A. N. Morozov, H. Auradou, *et al.*, A combined rheometry and imaging study of viscosity reduction in bacterial suspensions, *Proceedings of the National Academy of Sciences* **117**, 2326 (2020).
- [61] K. Drescher, R. E. Goldstein, N. Michel, M. Polin, and I. Tuval, Direct measurement of the flow field around swimming microorganisms, *Physical Review Letters* **105**, 168101 (2010).
- [62] D. O. Pushkin and J. M. Yeomans, Fluid mixing by curved trajectories of microswimmers, *Physical review letters* **111**, 188101 (2013).
- [63] K. Drescher, J. Dunkel, L. H. Cisneros, S. Ganguly, and R. E. Goldstein, Fluid dynamics and noise in bacterial cell-cell and cell-surface scattering, *Proceedings of the National Academy of Sciences* **108**, 10940 (2011).

- [64] M. M. Mrokowska, A. Krztoń-Maziopa, and M. Dbowski, Effect of exopolymer gels on the viscoelasticity of mucus-rich saltwater and settling dynamics of particles, *Marine Chemistry* **246**, 104163 (2022).
- [65] M. G. Mazza, The physics of biofilms an introduction, *Journal of Physics D: Applied Physics* **49**, 203001 (2016).
- [66] H. N. Ulloa and J. A. Letelier, Energetics and mixing of thermally driven flows in Hele-Shaw cells, *Journal of Fluid Mechanics* **930**, A16 (2022).
- [67] I. A. Houghton and J. O. Dabiri, Alleviation of hypoxia by biologically generated mixing in a stratified water column, *Limnology and Oceanography* **64**, 2161 (2019).
- [68] B. Fernandez Castro, M. Peña, E. Nogueira, M. Gilcoto, E. Broullón, A. Comesaña, D. Bouffard, A. C. Naveira Garabato, and B. Mourinho-Carballido, Intense upper ocean mixing due to large aggregations of spawning fish, *Nature Geoscience* **15**, 287 (2022).
- [69] R. V. More and A. M. Ardekani, Motion in stratified fluids, *Annual Review of Fluid Mechanics* **55**, 157 (2023).
- [70] J. Tamayo, Y. Zhang, M. E. Asp, A. Patteson, A. M. Ardekani, and A. Gopinath, Swarming bacterial fronts: Dynamics and morphology of active swarm interfaces propagating through passive frictional domains, *Biophysical Journal* **123**, 541a (2024).
- [71] D. Bárdfalvy, V. Škultéty, C. Nardini, A. Morozov, and J. Stenhammar, Collective motion in a sheet of microswimmers, *arXiv preprint arXiv:2310.05554* (2023).
- [72] D. Mondal, A. G. Prabhune, S. Ramaswamy, and P. Sharma, Strong confinement of active microalgae leads to inversion of vortex flow and enhanced mixing, *Elife* **10**, e67663 (2021).
- [73] G. T. Fortune, E. Lauga, and R. E. Goldstein, Biophysical fluid dynamics in a petri dish, *bioRxiv*, 2024 (2024).
- [74] A. Théry, L. Le Nagard, J.-C. Ono-dit Biot, C. Fradin, K. Dalnoki-Veress, and E. Lauga, Self-organisation and convection of confined magnetotactic bacteria, *Scientific Reports* **10**, 13578 (2020).
- [75] M. Akashi, T. Yanagisawa, Y. Tasaka, T. Vogt, Y. Murai, and S. Eckert, Transition from convection rolls to large-scale cellular structures in turbulent rayleigh-bénard convection in a liquid metal layer, *Physical Review Fluids* **4**, 033501 (2019).
- [76] D. Noto, H. N. Ulloa, and J. A. Letelier, Reconstructing temperature fields for thermally-driven flows under quasi-steady state, *Experiments in Fluids* **64**, 74 (2023).
- [77] A. J. Mathijssen, M. Lisicki, V. N. Prakash, and E. J. Mossige, Culinary fluid mechanics and other currents in food science, *Reviews of Modern Physics* **95**, 025004 (2023).
- [78] V. Mohit, A. Culley, C. Lovejoy, F. Bouchard, and W. F. Vincent, Hidden biofilms in a far northern lake and implications for the changing arctic, *npj Biofilms and Microbiomes* **3**, 17 (2017).
- [79] A. M. Anesio, S. Lutz, N. A. Christmas, and L. G. Benning, The microbiome of glaciers and ice sheets, *npj Biofilms and Microbiomes* **3**, 10 (2017).
- [80] A. de la Fuente, Heat and dissolved oxygen exchanges between the sediment and water column in a shallow salty lagoon, *Journal of Geophysical Research: Biogeosciences* **119**, 596 (2014).
- [81] T. J. Battin, K. Besemer, M. M. Bengtsson, A. M. Romani, and A. I. Packmann, The ecology and biogeochemistry of stream biofilms, *Nature Reviews Microbiology* **14**, 251 (2016).
- [82] N. Figueroa-Morales, L. Dominguez-Rubio, T. L. Ott, and I. S. Aranson, Mechanical shear controls bacterial penetration in mucus, *Scientific reports* **9**, 9713 (2019).
- [83] G. E. Flores, S. T. Bates, J. G. Caporaso, C. L. Lauber, J. W. Leff, R. Knight, and N. Fierer, Diversity, distribution and sources of bacteria in residential kitchens, *Environmental microbiology* **15**, 588 (2013).
- [84] M. Novak Babič, C. Gostinčar, and N. Gunde-Cimerman, Microorganisms populating the water-related indoor biome, *Applied microbiology and biotechnology* **104**, 6443 (2020).